Bulletin of Geophysics and Oceanography Vol. 66, n. 2, pp. 147-158; June 2025
DOI 10.4430/bgo00490

Water transport in the Earth's mantle: first evidence from seismograms of southern Tyrrhenian earthquakes

T. Ninivaggi[1], G. Selvaggi[2], S. Mazza[2], M. Filippucci[2,3], F. Tursi[4] and W. Czuba[5]

[1] *INGV, Istituto Nazionale di Geofisica e Vulcanologia, Sezione Irpinia, Grottaminarda, Italy*
[2] *INGV, Istituto Nazionale di Geofisica e Vulcanologia, ONT, Roma, Italy*
[3] *Dipartimento di Scienze della Terra e Geoambientali, Università degli Studi di Bari "Aldo Moro", Bari, Italy*
[4] *Dipartimento di Scienze della Terra, Università degli Studi di Torino, Torino, Italy*
[5] *Institute of Geophysics, Polish Academy of Sciences, Warsaw, Poland*

(Received: 12 September 2024; accepted: 1 April 2025; published online: 23 May 2025)

ABSTRACT An unknown later seismic phase has been found on waveforms of intermediate-depth and deep earthquakes of the southern Tyrrhenian subduction system. The later phase, called the x-phase, is a compressional wave, which leaves the source travelling downwards and propagating in the deepest edge of the Ionian lithosphere. It is, then, transmitted to the surface and observed at stations towards north, hundreds of kilometres away, appearing few seconds after the direct P wave. The observation of the x-phase and its peculiar seismological features have implications on the petrology of the Ionian slab and on water transport in the upper mantle. An additional aspect, to be further explored, is the possible presence of a similar later arrival after the S waves, which may add more information about the origin of the waves. This paper introduces previous findings and presents new analyses on S waves, completing earlier results and interpretations.

Key words: later seismic arrival/phase, waveform analyses, intermediate and deep seismicity, southern Tyrrhenian subduction zone, mineral phase A, DHMS phases.

1. Introduction

P and S waves reflected, refracted, or converted from deep earthquakes, known as later phases, have been widely used to constrain geometric characteristics of the Earth interior and, in particular, of subducting slabs (Zhao *et al*., 1997). Later phases could also be exploited to retrieve insights on the petrology and hydration conditions of a subducted lithosphere (Abers, 2000). A later seismic phase has been found in seismograms of European seismic stations from intermediate-depth and deep earthquakes of the southern Tyrrhenian subduction system and its origin is discussed in the work of Ninivaggi *et al*. (2023). The observation of later arrivals, as well as stimulating more in-depth analysis of raw seismograms, enables to draw hypotheses on the deepest features of the southern Tyrrhenian slab, with implications on the transportation of water in the mantle.

The subduction of the Ionian lithosphere beneath the Calabrian arc and the Tyrrhenian Sea is marked by an intense intermediate and deep seismicity (Fig. 1) which defines a well-known NW-

dipping Wadati-Benioff plane from the Ionian Sea towards the central Tyrrhenian Sea (Latorre *et al*., 2022, 2023). The slab is seismically continuous only in its south-western part, beneath the Aeolian Islands (vertical section AB) while, in the north-eastern portion, along the Calabrian coasts, the slab is mostly aseismic between 100 and 200 km of depth (vertical section CD). The tomographic images depict a continuous slab down to 400 km in its south-western portion, and the gap in seismicity probably reflects a horizontal discontinuity in its north-eastern edge [Lucente *et al*. (1999), Chiarabba *et al*. (2008), Scarfi *et al*. (2018), among many others]. The magnitude of the largest earthquakes can be greater than 6.0 and the greatest ever recorded occurred in 1938 with a magnitude of 7.0 (Anderson and Jackson, 1987). These earthquakes are well recorded at all European seismic stations.

In the work of Ninivaggi *et al*. (2023), the new later phase (called x-phase) is described and analysed. The x-phase arrives at stations located some hundreds of kilometres away from the epicentre towards north a few seconds after the direct P wave, and disappears at stations located in central and northern Europe. It is a P wave reaching the surface at stations from 650 to 950 km from epicentres, towards north. Among all the 43 analysed earthquakes that occurred in the southern Tyrrhenian subduction system between 1990 and 2020, with magnitude $M_L \geq 4.5$, only 12 earthquakes beneath the Aeolian Islands and in the depth range of 215 to 350 km show this later P-wave arrival. The x-phase arrives about 10 s after the direct P wave at epicentral distances of 650 km, and this difference decreases with increasing distances until the x-phase arrival disappears and only the first P-wave arrival is visible. The x-phase, therefore, follows its own travel-time curve with an apparent velocity of 11 km/s, higher than the first P-wave arrival. The robust observations and the seismological constraints derived from this analysis enabled Ninivaggi *et al*. (2023) to design a simple two dimensional (2D) velocity model to fit the x-phase arrival times. The model is designed in the vertical profile AB in Fig. 1, where all the earthquakes with the x-phase are located. The slab boundaries are based on seismicity. Outside the slab is the IASP91 velocity model (Kennett and Engdahl, 1991). The arrivals of the direct P wave are well fitted by a subducting lithosphere with an average increment of 1.5% of the IASP91 velocity model, whereas the x-phase requires much faster velocities, at least 3% higher than IASP91. Hence, Ninivaggi *et al*. (2023) introduced a high velocity layer (HVL) in the region where the earthquakes with the x-phase occurred. The HVL has an average increase of velocity up to 3% with respect to IASP91. Following Pino and Helmberger (1997), the 410-kilometre discontinuity is raised up to a depth of 370 km, as generally observed in subduction zones (Collier *et al*., 2001). This model can fit the x-phase arrival times for all the deep earthquakes below the Aeolian Island. According to the final model, the x-phase is interpreted as a compressional wave that propagates downwards in a HVL located in the subducted lithosphere and reflected from a shallower 410-kilometre discontinuity, located at 370 km of depth. A simple 2D modelling in Ninivaggi *et al*. (2023) shows, therefore, that a combination of velocity structure and geometric characteristics is able to reproduce rather well the observations of the whole data set. The author related the x-phase observation to the presence of a dense hydrous magnesium silicate phase A within the deepest edge of the slab, as the velocity value inside the HVL and its depth (from ~200 km to ~350 km) coincide with the stability of this mineral. The existence of the geochemical phase A is inferred from petrological laboratory experiments, and predicted in cold subduction zones (Van Keken *et al*., 2011; Cai *et al*., 2021).

All the analyses in Ninivaggi *et al*. (2023) were conducted on the time window in which the direct P wave arrives, as the new observed later arrival appears a few seconds after. As the nature of the x-phase is compressional (naming it henceforth the xp-phase), the earlier study mainly investigated the vertical component of seismic stations, mentioning the fact that a

transverse component of the x-phase is observed in some stations. In this work, we explore transverse components of the xp-phase and direct S waves, finding a later arrival after them. Our investigation holds the main conclusion dissertated in the previous work, adding new analyses previously not considered.

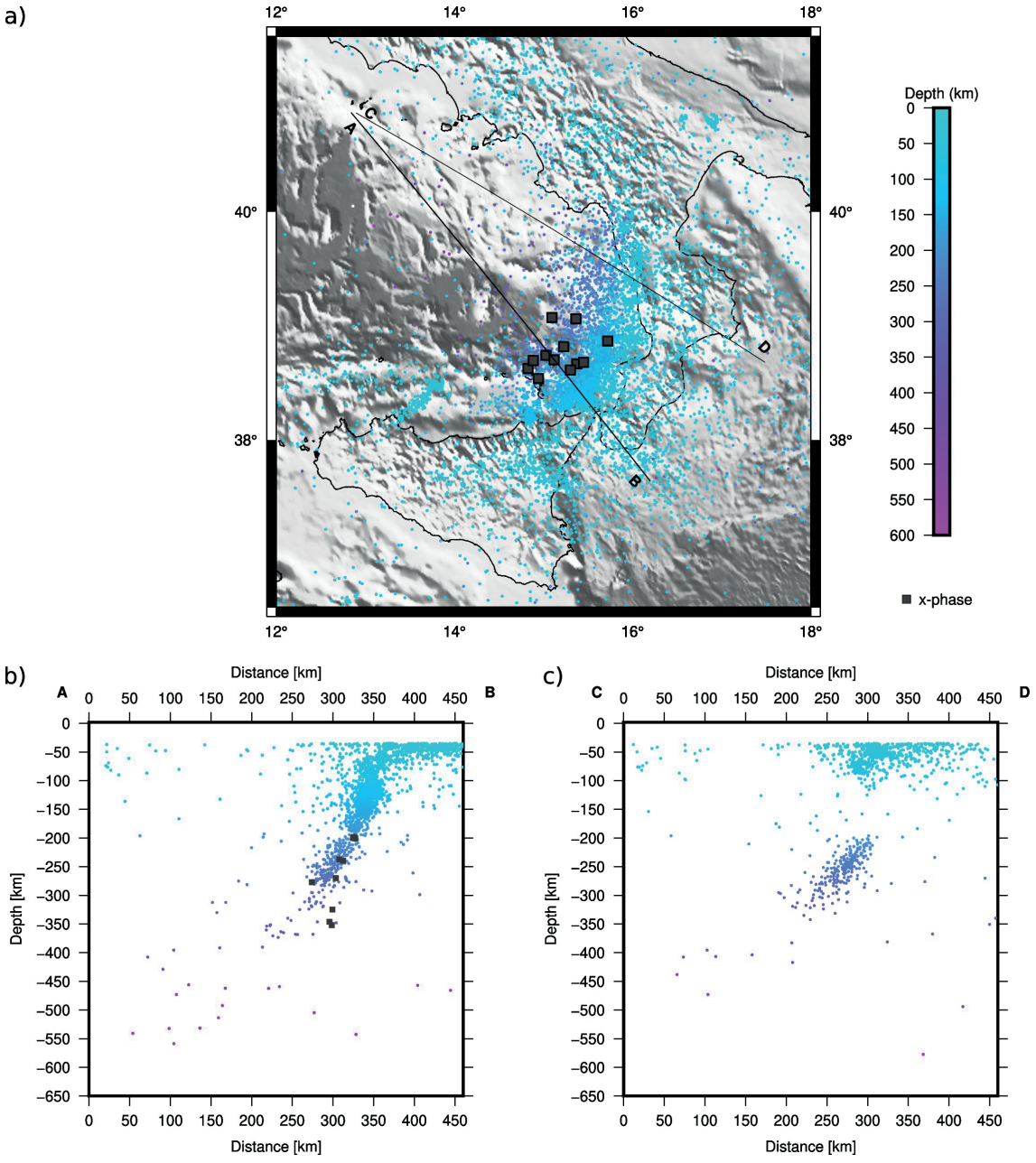

Fig. 1 - Seismicity map of the southern Tyrrhenian subduction zone from the catalogue of absolute (nonlinear) three dimensional (3D) earthquake locations from 1981 to 2018, depths greater than 35 km [CLASS: Latorre *et al*. (2022, 2023)]: a) grey filled squares are earthquakes where the x-phase has been recognised; b) vertical cross-sections perpendicular to the strike of the south-western part of the slab (AB), and c) slab's north-eastern part (CD).

2. Data and methods

We have inspected the largest intermediate-depth and deep earthquakes of the southern Tyrrhenian subduction system which occurred from 1990 to 2020 and shown the xp-phase. Such earthquakes are 12 and have a magnitude $M_L \geq 4.5$ and depths ranging from 215 to 350 km. They have been identified in the study of Ninivaggi *et al*. (2023) and are located in a well-defined region of the subducting Ionian lithosphere, with epicentres located in the eastern side of the Aeolian Arc [grey squares in Fig. 1, from CLASS (Latorre *et al*., 2022, 2023)]. We have considered broadband high gain seismometers (HH or BH streams) for each earthquake, when available. When they were not, we used short period high gain seismometers (EH or SH), especially for the oldest earthquakes. Seismic stations are from 0° to about 12° of distance from the selected epicentre (being the x-phase observed up to 9°), and cover a circular area from northern Africa to central Germany and between eastern Spain and Greece. Digital waveforms are downloaded from the European Integrated Data Archive (http://eida.ingv.it/) and from the Incorporated Research Institutions for Seismology Data Management Centre (https://service.iris.edu/). Most of the data are from the networks having identifiers IV, MN, NI, SI, SL, CH, GU, OE, and GR (University of Genoa, 1967; Federal Institute for Geosciences and Natural Resources, 1976; Swiss Seismological Service, 1983; ZAMG, 1987; Slovenian Environment Agency, 1990; MedNet Project Partner Institutions, 1990; OGS and UniTS, 2002; INGV, 2005).

The map in Fig. 2 shows an example of the seismic stations analysed for an earthquake, which

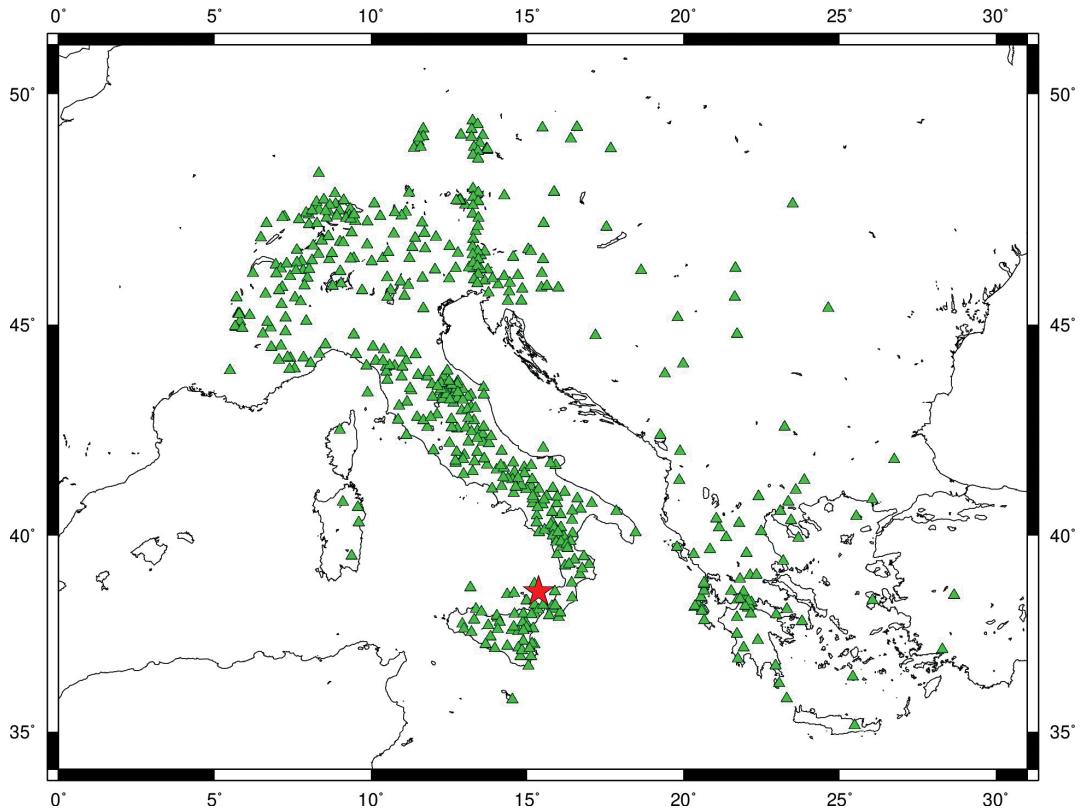

Fig. 2 - Seismic stations available (green triangles) for one of the analysed earthquakes, which occurred on 9 May 2015 at 08:22:41 at a depth of 214 km (red star).

occurred in 2015 at a depth of 215 km.

We have exploited classical methods of seismology to detect an eventual exotic seismic phase after S waves, visually inspecting waveforms, as in Ninivaggi *et al*. (2023). These methodologies include the identification and timing of seismic phases on seismograms (P, S, and later phases), the analysis of frequency content and particle motion. To investigate the later phase arrival times with increasing distance, a useful tool is the record section, on which the waveforms are sorted by distances and aligned by first arrivals (P or S waves), to exalt the later arrivals. They could also show the apparent velocity of seismic phases, which enable us to compare the velocities of the medium crossed by different waves. We have also investigated horizontal components, by analysing the transverse components of the xp-phase. These analyses are necessary to corroborate the previous interpretation on the origin of the observed later phases, adding new information to augment the value of previous results.

3. Results and interpretation

By analysing waveforms, we have found a later arrival after direct S waves, naming it the xs-phase. As shown in Fig. 3, the xs-phase arrives about 15 s after the direct S wave and 10 s before the reflected S wave at the 410-kilometre discontinuity in the upper mantle (S410s), at station MSSA, located 800 km from the epicentre. The later arrival has a frequency content of about

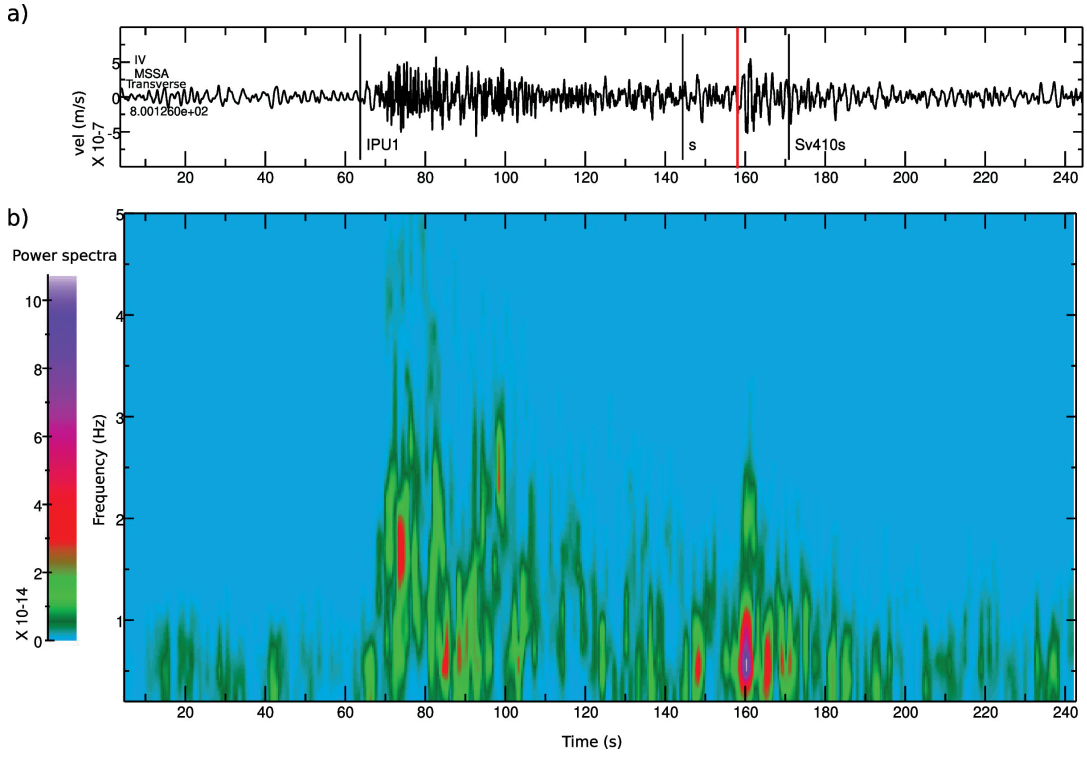

Fig. 3 - Transverse waveform and spectrogram of station MSSA [network IV, (INGV, 2005)] located at 800 km from the earthquake that occurred in 2015: a) tangential component in which the black vertical lines show, respectively, the calculated direct P wave, the direct S wave, and the S410s (the red vertical line indicates the xs-phase arrival); b) spectrogram of the seismogram.

1 Hz, which is slightly higher than that of the direct S waves (~0.5 Hz). Upon inspection of the three components of a single station, as shown in Fig. 4, the xs-wave is well distinguished in the tangential component, arriving at station PCP, located at 870 km from the epicentre, 15 s after the direct S wave and approximately 8 s earlier than the S410s. It has a particle motion mainly oriented in the transverse direction.

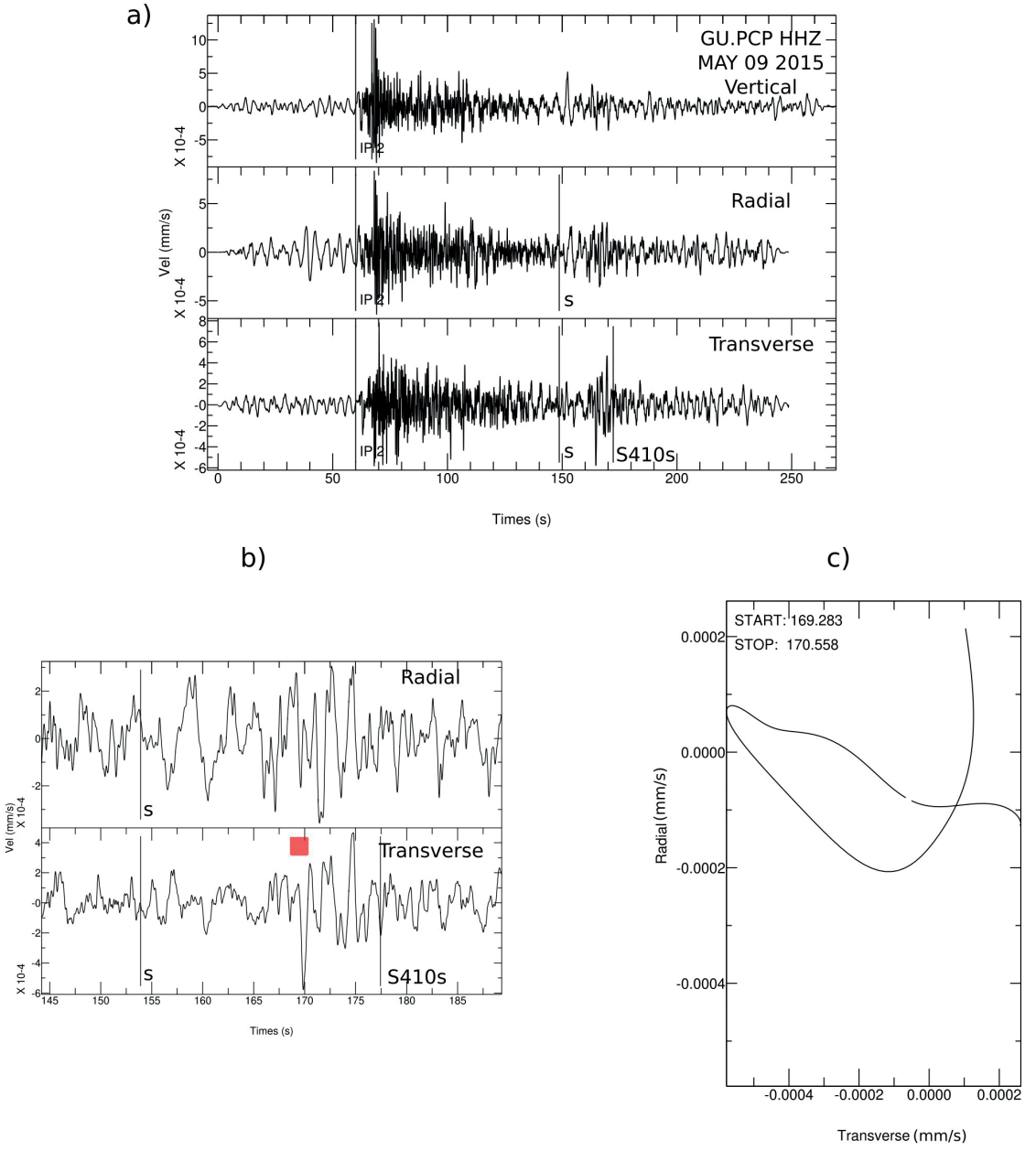

Fig. 4 - Waveforms and particle motion of the xs-phase: a) waveforms recorded by station PCP [network code GU, University of Genoa (1967)], distant 870 km from the 2015 earthquake (vertical lines show the calculated arrival time of the direct P wave, the direct S wave, and the S410s); b) zoom on the radial and transverse component on the S wave (the red square shows the later arrival); c) particle motion of the later wave.

Xs-phase recognition in the selected data set is performed through the visual inspection of the record sections, in which waveforms are sorted by epicentral distances. Fig. 5 shows the later arrival after direct S waves in a tangential record section, in the azimuthal range of 300° to 345°. Each horizontal waveform is normalised by its absolute maximum of amplitude and aligned by direct S waves, after it has been rotated in the transverse direction (perpendicular to the radial direction). The arrival precedes the S410s and is visible at epicentral distances from about 750 km to 1100 km. The travel time difference between the direct S wave and the xs-phase roughly decreases with increasing distances. However, the xs-phase is much less detectable than the xp-phase. Some waveforms do not have the later arrival (e.g. stations IV.CTI and SI.LUSI) but they also do not show a clear direct S-wave arrival. The apparent velocity is about 4.5 km/s for the direct S waves and about 5.5 km/s for the xs-phase. The latter probably crosses a medium that is deeper and with a higher propagation velocity compared to the direct S wave.

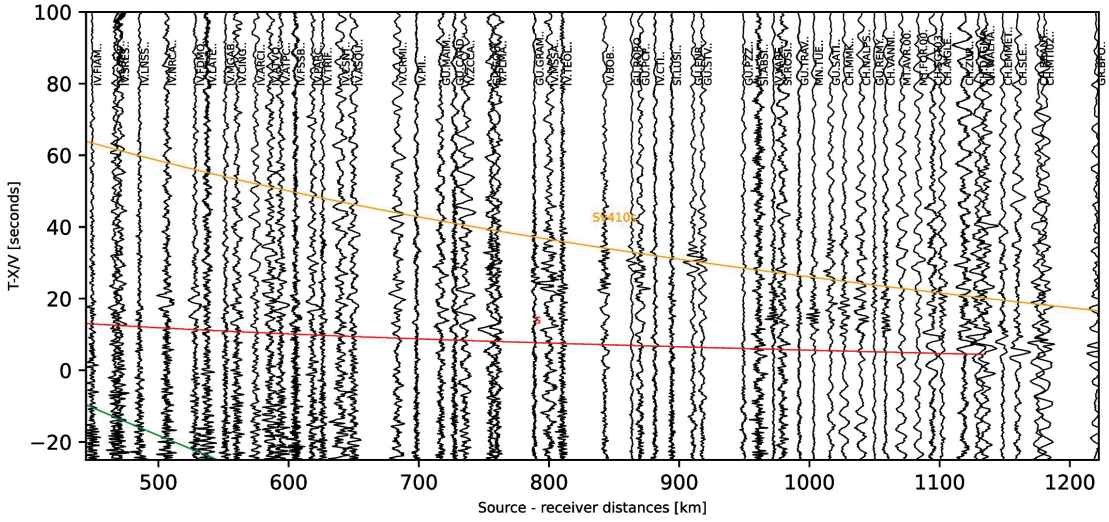

Fig. 5 - Transverse record section of the 2015 earthquake (9 May at 08:22:41, at a depth of 214 km, shown in Fig. 2). The waveforms are aligned with reduced time *T-X/V*, where *T* is the time from origin, *X* is the epicentral distance and *V* = 4.5 km/s, the apparent velocity of the direct S wave. The waveforms are in the azimuthal range of 300° to 345°. The red curve is the calculated direct S wave, the yellow curve is the reflected S wave at a 410-kilometre discontinuity (S410s).

We also performed new analyses to strengthen the seismological characteristics of the xp-phase. We checked the earthquakes with the xp-phase by analysing radial and tangential components. Fig. 6 shows three record sections of the earthquake that occurred in 2015 at a depth of 214 km. As shown in the plot, the xp-phase is also visible in the radial and tangential components. In the three record sections, the xp-phase amplitude and frequency content is higher than the direct P wave and the travel time difference between the direct P and xp decreases as the epicentral distances increase. The xp-phase amplitude is greater in the vertical and radial component, compared to the transverse one. In most cases, the xp-phase arrival is rather complicated as it is composed of multiple subsequent phases, as shown in Fig. 7. In the previous analysis of Ninivaggi *et al*. (2023), the authors have considered the first arrival after the direct P wave that emerged from the direct P coda (which is marked by the vertical line "x" in Figs. 7a and 7b). As we can see from Figs. 7c and 7d, however, the particle motion of the

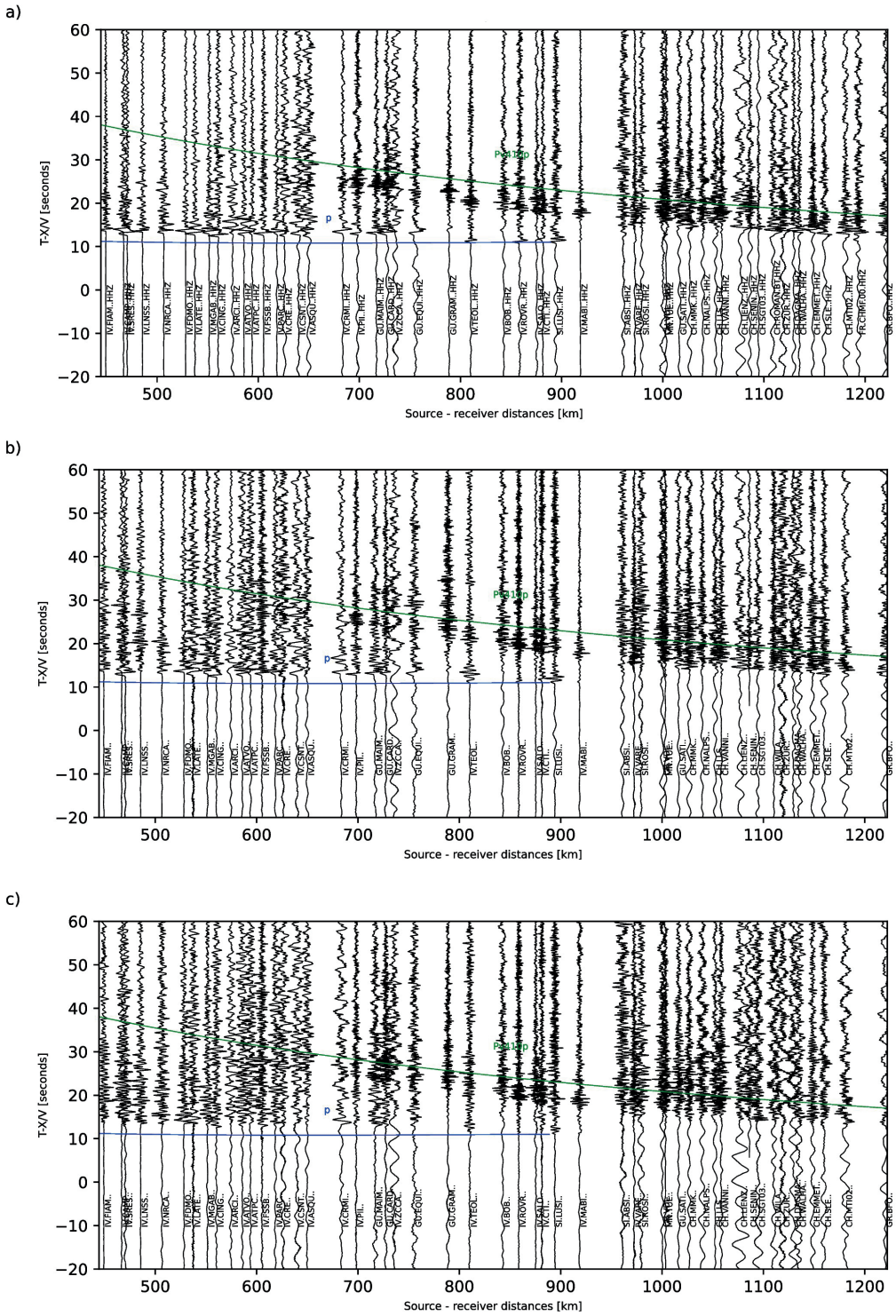

Fig. 6 - Record sections of the 2015 earthquake (location and origin time in the caption of Fig. 2). Waveforms are aligned by reduced time *T-X/V*, where *T* is the time from origin, *X* is the epicentral distance and *V* = 8.7 km/s is the apparent velocity of the direct P wave. Waveforms are in the azimuthal range of -60° to 30°.The blue line is the calculated direct P wave, the green one is the reflected P wave at a 410-kilometre discontinuity in the upper mantle (P410p). Each record section shows: a) vertical, b) radial, and c) transverse seismograms.

first x arrival and the following second phase, with greater amplitude, both display a vibration which is mainly oriented in the radial direction. In some cases, the second or the third wave (following the first x arrival) shows a particle motion oriented in the transverse direction or which is elliptical (Fig. 7e).

Following the new analyses, we can remark the previous interpretation of the xp-phase, which is a P wave travelling downwards in the deepest portion of the subducting plate. It is characterised by higher velocities of propagation and lower attenuation compared to those of the medium crossed by the direct P wave. The strong lateral and vertical heterogeneities of the subduction system probably cause the polarisation of the seismic wave also in the tangential direction. The xs-phase following the direct S wave, similarly to the xp-phase, probably leaves the source travelling downwards and crosses the same medium that the xp-phase crosses, reaching the surface on almost the same distance and azimuthal intervals of the xp-phase.

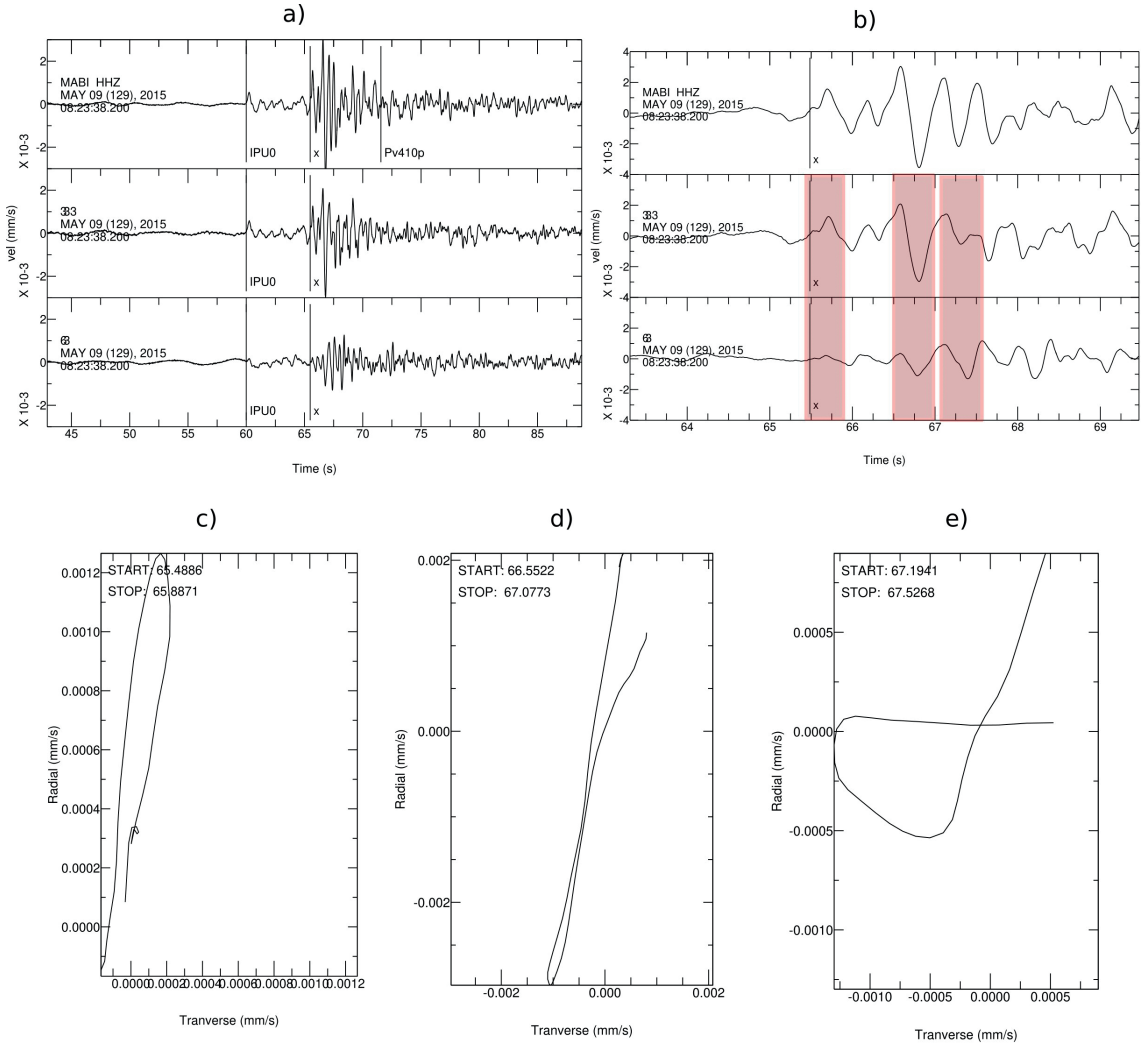

Fig. 7 - Waveforms and particle motion of the xp-phase: a) vertical, radial, and transverse components of station MABI (network code IV) at 918 km from the epicentre and b) zoom on the xp-phase arrival. The red rectangles in panel b show the time windows for which the particle motion is computed in panels c, d, and e.

4. Discussion and conclusions

The seismological constraints derived by Ninivaggi *et al*. (2023) could be completed with the new observations made in this study. The seismological features derived for the xs-phase are very similar to those of the xp-phase. Both later phases have a greater amplitude and frequency content than the direct phases (P or S). The xs-phase probably crosses a deeper and less attenuating medium compared to the direct S wave. The xs-phase arrives 15 s after the direct S wave and 10 s before the S410s. The S410s is the first (in time) observable wave in that time window, after the direct S wave, according to global travel time tables from a one dimensional velocity model (e.g. Kennett and Engdahl, 1991) and for deep earthquakes. The xs-phase could be considered as an unknown seismic phase, just as the xp-phase. The travel time curve followed by the xs-phase is similar to the xp-phase. The former appears at 750 km of distance from the epicentre and disappears at 1100 km towards north, in the azimuthal interval of 300°-350°. The xp-phase appears from 650 to 950 km of distance and in the azimuthal range of -60° to 30°, towards north. The travel time difference between the xs-phase and the direct S wave decreases as the distance increases, as do the xp-phase and its corresponding direct P wave. The xs-phase is observed on intermediate-depth and deep earthquakes of the southern Tyrrhenian subduction system, located below the eastern side of the Aeolian Arc in the depth range from 215 to 350 km. The xs-phase, therefore, could be considered an 'exotic' phase, originated by a peculiar 2D structure and related to the subduction system, just as the xp-phase. In the work of Ninivaggi *et al*. (2023), the xp-phase is interpreted as a compressional wave that propagates downwards in a HVL located in the subducted lithosphere and reflected from a shallower 410-kilometre discontinuity, located at 370 km of depth. It is reasonable to think that S waves, which propagate downwards, are also influenced by the slab and HVL, and that the latter could produce the later arrivals also after the direct S wave.

P-wave velocities inside the HVL range from 8.7 to 9.1 km/s at 300-350 km of depth. A simple explanation for the high velocity values of the HVL at such depths comes from petrology. In a cold subduction system (e.g. Groppo *et al*., 2016; Tursi *et al*., 2020; Wang *et al*., 2020), hydrated mafic-ultramafic rocks, which are deeply subducted, stabilise the dense hydrous magnesium silicates (DHMS) (e.g. Irifune *et al*., 1998) in their mineral assemblages. These rocks, previously exposed at the ocean floor, enter into the subduction zone as locally hydrated, with water incorporated into OH-bearing minerals (Hacker *et al*., 2003a, 2003b; Fumagalli and Poli, 2005; Fumagalli *et al*., 2014; Hermann and Lakey, 2021). The DHMS mineral phases contain up to 18 wt% of water, so they influence the deep water-cycle in the mantle (Irifune *et al*., 1998; Komabayashi, 2004; Maurice *et al*., 2018), thus, playing a crucial role in the evolution of the Earth (Bercovici and Karato, 2003). The breakdown of hydrated minerals, also, has geodynamic implications on subduction systems, triggering earthquakes via a process of dehydration embrittlement (Fumagalli and Poli, 2005). Phase A is the earliest of the DHMS which becomes stable at depths greater than 200 km, replacing antigorite after its breakdown (Sclar *et al*., 1965; Iwamori, 2004, among the others), in cold subduction systems. In the upper-mantle deep slab, phase A is the dominant hydrous phase for water transportation into deep Earth (Cai *et al*., 2021). Recent ultrasonic measurements of compressional wave velocities inside mineral phase A (Cai *et al*., 2021) show values comparable to the P-wave velocities that Ninivaggi *et al*. (2023) introduced in the HVL model to explain the xp-phase observations. Also, the depth of the HVL, together with the depths of the earthquakes with both xp and xs later phases, are compatible with the depth stability of phase A. We have, therefore, interpreted the HVL and the observation of both later phases (xp and xs), as intimately related to the presence of mineral phase A in the site of the Tyrrhenian subduction system.

Acknowledgments. The paper includes new analysis which completes the work presented at the 42nd National Conference of the GNGTS, "Geophysics for the future of the Planet", 13-16 February 2024, Ferrara, Italy. We would like to thank the convenors Anna Maria Marotta, Carla Braitenberg, and Barbara Orecchio, along with the anonymous reviewers, for their enlightening comments. We also thank the Editor-in-Chief, Dario Slejko, for his suggestions. This work has been funded by INGV internal funding (Bando Ricerca Libera 2019) and supported by a subsidy from the Polish Ministry of Education and Science for the Institute of Geophysics, Polish Academy of Sciences.

REFERENCES

Abers G.A.; 2000: *Hydrated subducted crust at 100–250 km depth*. Earth Planet. Sci. Lett., 176, 323–330, doi: 10.1016/S0012-821X(00)00007-8.

Anderson H. and Jackson J.; 1987: *The deep seismicity of the Tyrrhenian Sea.* Geophys. J. R. Astr. Soc., 91, 613-637, doi: 10.1111/j.1365-246X.1987.tb01661.x.

Bercovici D. and Karato S.-I.; 2003: *Whole-mantle convection and the transition-zone water filter*. Nature, 425, 39–44, doi: 10.1038/nature01918.

Cai N., Qi X., Chen T., Wang S., Yu T., Wang Y., Inoue T., Wang D. and Li B.; 2021: *Enhanced visibility of subduction slabs by the formation of dense hydrous phase A*. Geophys. Res. Lett., 48 (19), 1–10, doi: 10.1029/2021GL095487.

Chiarabba C., De Gori P. and Speranza F.; 2008: *The southern Tyrrhenian subduction zone: deep geometry, magmatism and Plio-Pleistocene evolution*. Earth Planet. Sci. Lett., 268, 408–423, doi: 10.1016/j.epsl.2008.01.036.

Collier J.D., Helffrich G.R. and Wood B.J.; 2001: *Seismic discontinuities and subduction zones*. Phys. Earth Planet. Inter., 127, 35–49, doi:10.1016/S0031-9201(01)00220-5.

Federal Institute for Geosciences and Natural Resources; 1976: *German Regional Seismic Network (GRSN)*. Bundesanstalt für Geowissenschaften und Rohstoffe, doi: 10.25928/mbx6-hr74.

Fumagalli P. and Poli S.; 2005: *Experimentally determined phase relations in hydrous peridotites to 6.5 GPa and their consequences on the dynamics of subduction zones.* J. Petrol, 46, 555–578. doi: 10.1093/petrology/egh088.

Fumagalli P., Poli S., Fischer J., Merlini M. and Gemmi, M.; 2014: *The high-pressure stability of chlorite and other hydrates in subduction mélanges: experiments in the system Cr_2O_3-MgO-Al_2O_3-SiO_2-H_2O*. Contrib. Mineral. Petrol., 167, doi: 10.1007/s00410-014-0979-5.

Groppo C., Rolfo F., Sachan H.K. and Rai S.K.; 2016: *Petrology of blueschist from the western Himalaya (Ladakh, NW India): exploring the complex behavior of a lawsonite-bearing system in a paleo-accretionary setting*. *Lithos*, *252*, 41-56, doi: 10.1016/j.lithos.2016.02.014.

Hacker B.R., Abers G.A. and Peacock S.M.; 2003: *Subduction factory 1. Theoretical mineralogy, densities, seismic wave speeds, and H_2O contents*. J. Geophys. Res. Solid Earth, 108 (B1), doi: 10.1029/2001jb001127.

Hacker B.R., Peacock S.M., Abers G.A. and Holloway S.D.; 2003: *Subduction factory 2. Are intermediate-depth earthquakes in subducting slabs linked to metamorphic dehydration reactions?* J. Geophys. Res. Solid Earth, 108 (B1), doi: 10.1029/2001jb001129.

Hermann J. and Lakey S.; 2021: *Water transfer to the deep mantle through hydrous, Al-rich silicates in subduction zones.* Geology, 49, 911–915, doi: 10.1130/G48658.1.

INGV (Istituto Nazionale di Geofisica e Vulcanologia); 2005: *Rete Sismica Nazionale (RSN) [Dataset].* Istituto Nazionale di Geofisica e Vulcanologia, Roma, Italy, doi: 10.13127/SD/X0FXNH7QFY.

Irifune T., Kubo N., Isshiki M. and Yamasaki Y.; 1998: *Phase transformations in serpentine and transportation of water into the lower mantle.* Geophys. Res. Lett., 25, 203–206, doi: 10.1029/97GL03572.

Iwamori H.; 2004: *Phase relations of peridotites under H_2O-saturated conditions and ability of subducting plates for transportation of H_2O.* Earth Planet. Sci. Lett., 227, 57–71, doi: 10.1016/j.epsl.2004.08.013.

Kennett B.L.N. and Engdahl E.R.; 1991: *Traveltimes for global earthquake location and phase identification.* Geophys. J. Int., 105, 429-465, doi: 10.1111/j.1365-246X.1991.tb06724.x.

Komabayashi T.; 2004: *Petrogenetic grid in the system MgO-SiO_2-H_2O up to 30 GPa, 1600° C: applications to hydrous peridotite subducting into the Earth's deep interior.* J. Geophys. Res., 109, doi: 10.1029/2003jb002651.

Latorre D., Di Stefano R., Castello B., Michele M. and Chiaraluce L.; 2022: *Catalogo delle Localizzazioni ASSolute (CLASS): locations (Version 1).* Istituto Nazionale di Geofisica e Vulcanologia, Roma, Italy, doi: 10.13127/class.1.0.

Latorre D., Di Stefano R., Castello B., Michele M. and Chiaraluce L.; 2023: *An updated view of the Italian seismicity from probabilistic location in 3D velocity models: the 1981–2018 Italian catalog of absolute earthquake locations (CLASS).* Tectonophysics, 846, doi: 10.1016/j.tecto.2022.229664.

Lucente F.P., Chiarabba C., Cimini G.B. and Giardini D.; 1999: *Tomographic constraints on the geodynamic evolution of the Italian region.* J. Geophys. Res. Solid Earth, 104 (B9), 20307–20327, doi: 10.1029/1999JB900147.

Maurice J., Bolfan-Casanova N., Padrón-Navarta J.A., Manthilake G., Hammouda T., Hénot J.M. and Andrault D.; 2018: *The stability of hydrous phases beyond antigorite breakdown for a magnetite-bearing natural serpentinite between 6.5 and 11 GPa.* Contrib. Mineral. Petrol., 173, doi: 10.1007/s00410-018-1507-9.

MedNet Project Partner Institutions; 1990: *Mediterranean Very Broadband Seismographic Network (MedNet) [Dataset]*. Istituto Nazionale di Geofisica e Vulcanologia, Roma, Italy, doi: 10.13127/sd/fbb td td 6q.

Ninivaggi T., Selvaggi G., Mazza S., Filippucci M., Tursi F. and Czuba W.; 2023: *Nature and origin of an undetected seismic phase in waveforms from southern Tyrrhenian (Italy) intermediate-depth and deep earthquakes: first evidence for the phase-A in the subducted uppermost lithospheric mantle?* Tectonophysics, 860, 229919, doi: 10.1016/j.tecto.2023.229919.

OGS and UniTS (Istituto Nazionale di Oceanografia e di Geofisica Sperimentale and University of Trieste); 2002: *North-East Italy Broadband Network [Dataset].* International Federation of Digital Seismograph Networks, doi: 10.7914/SN/NI.

Pino N.A. and Helmberger D.V.; 1997: *Upper mantle compressional velocity structure beneath the west Mediterranean basin.* J. Geophys. Res., 102 (B2), 2953–2967, doi: 10.1029/96JB03461.

Scarfì L., Barberi G., Barreca G., Cannavò F., Koulakov I. and Patanè D.; 2018: *Slab narrowing in the central Mediterranean: the Calabro-Ionian subduction zone as imaged by high resolution seismic tomography*. Sci. Rep., 8, doi: 10.1038/s41598.018-23543-8.

Sclar C.B., Carrison L.C. and Schwartz C.M.; 1965: *High-pressure synthesis and stability of a new hydronium-bearing layer silicate in the system MgO–SiO_2–H_2O.* Trans. Am. Geophys. Union, 46, 184.

Slovenian Environment Agency; 1990: *Seismic Network of the Republic of Slovenia [Dataset]*. International Federation of Digital Seismograph Networks, doi: 10.7914/SN/SL.

Swiss Seismological Service; 1983: *National Seismic Networks of Switzerland [Dataset]*. ETH, Zürich, Switzerland, doi: 10.12686/SED/NETWORKS/CH.

Tursi F., Bianco C., Brogi A., Caggianelli A., Prosser G., Ruggieri G. and Braschi E.; 2020: *Cold subduction zone in northern Calabria (Italy) revealed by lawsonite–clinopyroxene blueschists*. J. Metamorph. Geol., 38, 451-469, doi: 10.1111/jmg.12528.

University of Genoa; 1967: *Regional Seismic Network of North Western Italy [Dataset].* International Federation of Digital Seismograph Networks, doi: 7914/SN/GU.

Van Keken P.E., Hacker B.R., Syracuse E.M. and Abers G.A.; 2011: *Subduction factory: 4. Depth-dependent flux of H_2O from subducting slabs worldwide.* J. Geophys. Res., 116, doi: 10.1029/2010JB007922.

Wang H., Liu F., Santosh M., Cai J., Wang F. and Ji L.; 2020: *Rapid cold slab subduction of the Paleo-Tethys: Insights from lawsonite-bearing blueschist in the Changning–Menglian orogenic belt, southeastern Tibetan plateau*. Gondwana Research, 85, 189-223. doi: 10.1016/j.gr.2020.05.006.

ZAMG (Zentralanstalt für Meterologie und Geodynamik); 1987: *Austrian Seismic Network [Dataset].* International Federation of Digital Seismograph Networks, doi: 10.7914/SN/OE.

Zhao D., Matsuzawa T. and Hasegawa A.; 1997: *Morphology of the subducting slab boundary in the northeastern Japan arc*. Phys. Earth Planet. Inter., 102, 89–104, doi: 10.1016/S0031-9201(96)03258-X.

Corresponding author: Teresa Ninivaggi
INGV - Sezione di Milano
Via Alfonso Corti 12, 20133, Milano, Italy
Phone: +39 333 465 3060; e-mail: teresa.ninivaggi@ingv.it